

# Wrinkling of a Membrane with a Curved Small Thin Film

By Masanori MATSUSHITA,<sup>1)</sup> Osamu MORI,<sup>2)</sup> Nobukatsu OKUIZUMI,<sup>2)</sup>  
 Yasutaka SATOU,<sup>2)</sup> Takashi IWASA,<sup>3)</sup> and Saburo MATUNAGA<sup>4)</sup>

<sup>1)</sup>Department of Mechanical and Aerospace Engineering, Tokyo Institute of Technology, Tokyo, Japan

<sup>2)</sup>Institute of Space and Astronautical Science, JAXA, Sagami-hara, Japan

<sup>3)</sup>Department of Mechanical and Aerospace Engineering, Tottori University, Tottori, Japan

<sup>4)</sup>Department of Mechanical Engineering, School of Engineering, Tokyo Institute of Technology, Tokyo, Japan

(Received June 30th, 2017)

In the operation of a solar power sail IKAROS, curved thin-film solar cells were assumed to make the membrane deformed. The deformation caused propellant consumption to counteract windmill torque. For a next solar power sail in the Japan Aerospace Exploration Agency, we conducted experiments and finite element simulations of a simplified model of a part of the solar power sail to understand the effect of a small curved thin-film on wrinkles in a thin membrane under uniaxial tension force. We compared shapes of the membrane with the curved thin-film solar cell under varying tension force. Main findings are that wrinkle lines near both lateral sides of a small curved thin film are bended by curvature of the film and occur under varying tension force.

**Key Words:** Membrane Structures, Solar Sail, Thin-Film Device, Wrinkle

## Nomenclature

$E$	: Young's modulus
$F$	: force
$I$	: second moment of area
$M$	: moment
$\alpha$	: mass-proportional damping factor
$\beta$	: stiffness-proportional damping factor
$\rho$	: radius of curvature

## 1. Introduction

A solar power sail, which has a membrane with thin-film solar cells, IKAROS<sup>1)</sup> was demonstrated on orbit in 2010. In the actual operation, some phenomena related to the membrane occurred. One of them was a windmill effect. The windmill effect is that distortion of a sail reflecting photon flux causes in-plane torque. Because windmill torque disturbed the spin rate, the propellant was wasted to control the angular velocity. Therefore, this torque should be predicted. Another phenomenon was that deflection of the membrane induced by solar pressure under low spin rate (0.055 rpm) was smaller than expected. This indicates that the out-of-plane stiffness of the membrane was bigger than predicted. Satou et al.<sup>2)</sup> and Okuizumi et al.<sup>3)</sup> suggested that high out-of-plane stiffness can be caused by the increased bending stiffness due to the curved thin-film solar cells by finite element simulations. They also concluded that the propagation of wrinkles throughout the membrane is considered to be induced by curving thin-film solar cells. However, it is still unclear how the out-of-plane stiffness became higher and the membrane deflection grew. It is important to elucidate these mechanisms for a next generation solar power sail in the Japan Aerospace Exploration Agency (JAXA) (Fig. 1). The thin-film solar cell is curved unintentionally in the manufacturing process due to a bimetallic effect that is induced by layers of different metals of the cell. The spinning solar power sail has a polyimide

membrane of whole size 50 m × 50 m and thickness of 10 μm with a lot of thin-film solar cells. It is also important to build a simulation model of the membrane with the curved thin-film solar cells and evaluate the shape for the next solar power sail.

Although a lot of studies have investigated wrinkles in a thin membrane, few studies have investigated wrinkles in the membrane with small thin films. Wong et al.<sup>4)</sup> worked on wrinkled membrane without thin films, and many other researchers also have done. On the other hand, there are a few studies to control shape of a wrinkled membrane using thin-film devices. Senba et al.<sup>5)</sup> suggested temperature-induced shape memory polymer patches as actuators to control wrinkle and slack of a membrane. However, they did not focus on how curved thin films make wrinkles in a flat membrane.

In this paper, as a preliminary study, a part of the next solar power sail is simply modeled to investigate local wrinkles near the curved cell under varying uniaxial tension force as centrifugal force. The tension force was changed to investigate the relationship between the tension and deformation of the membrane with the curved film. Then, we simulated deformation of the model using a finite element model. Finally, the simulation results are verified using the measured shape of the membrane with the curved film. This work contributes to understand the effects of a curved small thin film on wrinkles near the curved film in a thin membrane under uniaxial tension force and to model the next solar power sail.

## 2. Simplified Model of a Part of Spinning Solar Power Sail

This section introduces a simplified model of a part of the spinning solar power sail. Based on this model, simulations and experiments in the following sections are conducted. This model provides a basis for modeling the global membrane of the solar sail. This model can also be applied to a basic model of deployable membrane structures with extendable masts, such as a roll-out solar array.<sup>6)</sup>

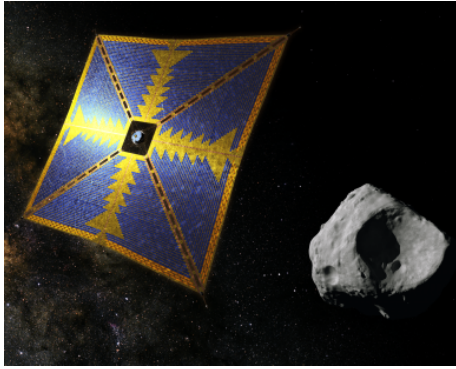


Fig. 1. Image of JAXA's next solar power sail to Jupiter Trojans.

Figure 2 shows a simplified model of a part of the spinning solar power sail. Bridges between trapezoidal petals and devices on the membrane except for thin-film solar cells are ignored for simplicity. Uniaxial tension force is adopted because radial force is more dominant than circumferential force in the spinning solar sail. In the simplified model, a thin-film solar cell is put on the center of the membrane surface. There are a curvature of the cell in the direction orthogonal to the force and no curvature in the direction along the force. The rectangle shape of the membrane is adopted because it is assumed that wrinkle occurs near the cell along tensile force. A matte polyethylene terephthalate (PET) membrane, Lumirror X42G is used to reduce optical transparency and specular reflection for three-dimensional (3D) scanning although Lumirror X42G thickness of  $50\ \mu\text{m}$  is different from the next solar sail membrane thickness of  $10\ \mu\text{m}$ . Note that the similarity rule between the next solar sail and the simplified model is not considered.

Relevant parameters in deformation of the membrane with the curved thin film include tension force, curvature, thickness, Young's modulus and Poisson's ratio. In this study, we changed tension force because the membrane of the spinning solar sail is kept flat by centrifugal force, which is easily changed by the unstable spin rate. The force is changed to 9800, 980, 98 and 9.8 mN (stress on the membrane is set to 1.96, 0.196, 0.0196 and 0.00196 MPa) in the simulations and experiments with reference to the IKAROS's criterion that spin rate is maintained at greater than 1 rpm, that is, the centrifugal force of 55 mN on a 0.5 kg tip mass during the normal operations although the force cannot simply be compared with the centrifugal force on the IKAROS. The centrifugal force was set to approximately 340 mN at the spin rate of 2.5 rpm in the actual nominal operation of the IKAROS.

### 3. Finite Element Model of a Part of Spinning Solar Power Sail

#### 3.1. Overview of finite element model

A finite element model of the membrane with the curved cell is shown in Fig. 3. An explicit dynamic, geometrically nonlinear finite-element software Abaqus/Explicit 6.14-2 was used. S4R thin-shell elements are used in the simulation model. The mesh size ( $1\ \text{mm} \times 1\ \text{mm}$ ) is sufficiently dense for convergence of shape for the following reasons: Several preliminary analyses, whose mesh sizes were  $0.5\ \text{mm} \times 0.5\ \text{mm}$ ,  $1\ \text{mm} \times 1\ \text{mm}$ ,  $2\ \text{mm} \times 2\ \text{mm}$  and  $4\ \text{mm} \times 4\ \text{mm}$ , were conducted and these

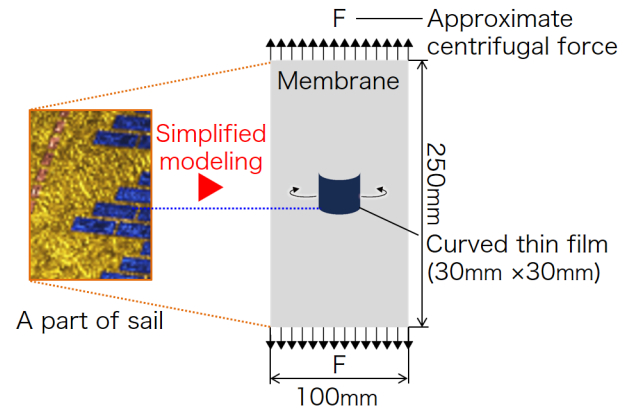


Fig. 2. Model of membrane with small thin film under tension force. This model is a simplified model of a part of the spinning solar power sail.

Table 1. Properties of PET membrane.

Properties	Values
Size (mm)	$100 \times 250$ (Measured value)
Thickness ( $\mu\text{m}$ )	$5.0 \times 10^1$ (Measured value)
Density ( $\text{g}/\text{cm}^3$ )	1.4 (Supplier's data)
Young's modulus (GPa)	4 (Supplier's data)
Poisson's ratio	0.3 (Assumed value)

Table 2. Properties of amorphous silicon thin-film solar cell.

Properties	Values
Size (mm)	$30 \times 30$ (Measured value)
Thickness ( $\mu\text{m}$ )	$5.8 \times 10^1$ (Measured value)
Density ( $\text{g}/\text{cm}^3$ )	1.4 (Measured value)
Young's modulus (GPa)	$2 \times 10^1$ (Measured value)
Poisson's ratio	0.3 (Assumed value)
Radius of curvature (mm)	$1.5 \times 10^1$ (Measured value)

shapes of the models were qualitatively the same; and Wong et al.<sup>7)</sup> said that a mesh density of about 6 elements over a whole wave length of a wrinkle was found sufficient to obtain accurate results. In the case of the chosen mesh size, there are 10 elements over the whole wave length even if 10 whole wrinkles occurred in the short direction.

A PET membrane, Lumirror X42G (Table 1) and an amorphous silicon thin-film solar cell (Table 2) are used in the simulations and experiments. The cell was adopted for the IKAROS. Initial geometrical imperfections are not introduced. A shell edge force  $F$  is used on the top side of the membrane. Shell edge moments  $M$  are also used on both lateral sides of the curved cell. The  $M$  of 0.61 mNm was calculated using the properties of the cell and the following bending-curvature equation

$$M = \frac{EI}{\rho}. \quad (1)$$

The results of the deformed shape are compared with the measured data in the following section. Since stress was not measured in the experiment, appearance of slack regions, which are unstable shape zones and can induce windmill torque, was investigated using maximum in-plane principle stress in the simulation. Checking the stress field in the sail is important in order to control windmill torque because slack regions can make shape of the membrane asymmetric.

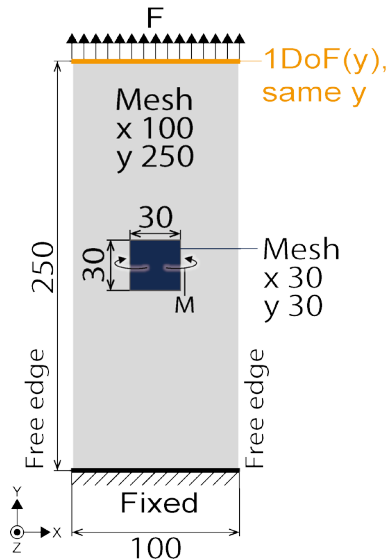


Fig. 3. Finite element model of membrane with curved thin film.

### 3.2. Constraints and boundary conditions

The back surface of the small thin film part is connected to the front surface of the membrane using a tie constraint. Boundary conditions of the membrane are as follows:

- The top side is allowed to move only in the y-direction, and nodes on the top side have the same y-position using a kinematic coupling constraint.
- Both the lateral side edges remain free.
- The bottom side is fully constrained.

### 3.3. Rayleigh damping and mass scaling

Rayleigh damping consisted of mass and stiffness proportional terms is used to afford numerical convergence. The Abaqus analysis user's guide states that large mass-proportional damping factor,  $\alpha$  is often undesirable, and stiffness-proportional damping factor,  $\beta$  should be less than or of the same order of magnitude as the initial stable time increment without damping.<sup>8)</sup> To meet the above criteria,  $\alpha$  and  $\beta$  are set to  $10^{-3} \text{ s}^{-1}$  and  $10^{-8} \text{ s}$ . Semi-automatic fixed mass scaling is adopted for the whole model, and the time increment is set to below 0.005 s.

### 3.4. Simulation steps

The simulation consists of two steps, as follows: In the first step, the shell edge moments on the both lateral side edges are increased in a ramp state. The first step time is 3,000 s. In the second step, the shell edge force is increased in a ramp state. The second step time is 10,000 s. The total step time is 13,000 s.

## 4. Experimental Method

### 4.1. Overview of experimental method

We measured shapes of a membrane with a curved thin-film cell under each tension to verify the simulation model. Figure 4 shows a schematic diagram of an experimental setup. The membrane with the cell was pulled by weights and fixed on a tension test apparatus. Then, the shape was measured using a 3D scanner. The details are shown in this section. The experiments were conducted under the ambient temperature of 20 degrees Celsius.

### 4.2. Membrane and thin film

The material properties of the membrane and the cell (Tables 1 and 2) were used. The PET membrane is matte because specular reflection is bad for optical scanning, which we selected a scanning type. The curved cell was put on the membrane with a room temperature vulcanization (RTV) silicone (SILASCON, Dow Corning Toray), which was used for the IKAROS. Radius of curvature of the cell was measured before adhesion of the cell to the membrane.

### 4.3. Fixation and tension method using tension test apparatus

We developed a tension test apparatus that enables to fix top and bottom edges of a membrane and adds uniaxial tension to the membrane (Fig. 5). The frame (560 mm  $\times$  590 mm) consists of aluminum extrusions (A6063S-T5, MISUMI). The way to fix and pull the membrane is as follows:

- The bottom edge of the membrane is clamped by a A6063 clamping strip.
- The top end of the membrane is fixed to an aluminum alloy bar fixed with a polyimide adhesive tape.
- The bar is inserted in rings of ultra-high molecular weight polyethylene cords (ULTRA2, YGK Yotsu Ami), which are connected with weights through pulleys.
- The top of the pulled membrane is clamped by the other clamping strip.

Double-sided tapes (NO.7643 #12, TERAOKA) are put on one surface of the clamping strips to reduce initial imperfections and fix the membrane. Adhesive strength of the double-sided tape is sufficiently strong to fix the pulled membrane even if the clamping strip is not used. Note that tension force on the membrane was not measured although the weights were measured.

### 4.4. Measurement method using 3D scanner

We used a commercial structured-light 3D scanner (SLS-3, DAVID) consisted of a projector, a charge coupled device (CCD) camera (1,920  $\times$  1,200 pixels) and a personal computer with a 3D scanner software (DAVID 5) to measure shape of the membrane. The structured-light 3D scanning is based on triangulation. The 3D scanner can measure positions but cannot measure displacements. Using the structured-light 3D scanner, a single scan can cover a wide range at one time within approximately 10 seconds. The distance between the CCD camera and the membrane are set to 43 cm because the distance should be short for high precision. At the distance, the 3D scanner was not able to measure the whole membrane at one time. Therefore, the top half and bottom half of the membrane were separately measured. The precision of 100  $\mu\text{m}$  was measured at the distance. The total number of raw 3D point data per scan is approximately 1,500,000. For data processing, the total data volume is reduced to 180,000. Then, the average spacing between 3D point data becomes approximately 0.4 mm.

## 5. Results and Discussion

In this section, out-of-plane position of the membrane with the curved cell in the simulations and experiments are compared to verify the simulation model. Maximum principal stress of the simulation model is shown and discussed to investigate shape stability.

In the simulations, the origin of coordinates is center of the

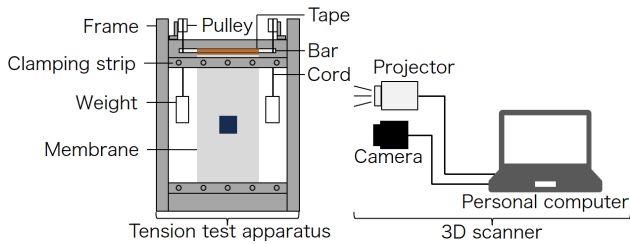


Fig. 4. Schematic diagram of experimental setup.

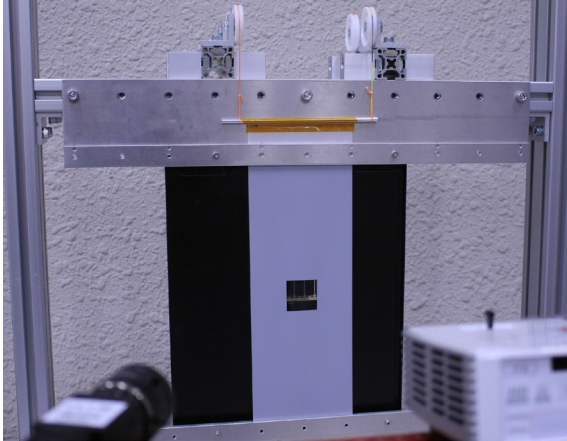


Fig. 5. Membrane with curved cell fixed on tension test apparatus.

membrane before deformation; a reference plane ( $z = 0$  mm) is a neutral plane of the membrane. Directions of the axes are shown in Fig. 3. In the experiments, the  $x$ -origin is the average of the measured membrane with the curved cell. The  $y$ -origin is 125 mm from the bottom edge of the membrane, which is center of the membrane before deformation. A reference plane ( $z = 0$  mm) is the average of measured  $z$ -position of the top and bottom edges of the membrane, which are hardly deformed.

### 5.1. Out-of-plane position

Figures 6, 7, 8, and 9 show contour plots of out-of-plane position,  $z$  of the membrane with the curved cell under each tension force in the simulations and experiments.  $Z$  of neutral planes of both the membrane and the curved cell in the simulations is plotted. The numerical shapes qualitatively match the measured shapes under each tension force. The X-shaped wrinkles occurred beside the cell in each contour plot because of the tension force and curvature of the cell. We also confirmed that parallel wrinkle lines occurred in a 10- $\mu$ m-thick polyimide membrane with a flat PET film under 9800 mN tension force.<sup>9)</sup> Therefore, it is suggested that curvature of the cell bends wrinkle lines beside the cell.

The global shape of the membrane under 9800 mN (Fig. 6) is different from those of the membrane under 980, 98 and 9.8 mN tension (Figs. 7, 8, and 9), that is, a wrinkle pattern changed between 9800 and 980 mN.

It is suggested that strong tension force of 9800 mN can reduce the effect of initial imperfections on deformation of the membrane. In the experiment under 9800 mN tension (Fig. 6(a)), the bottom area of the membrane is not distorted by initial imperfections of the clamped bottom edge. On the other hand, in the experiments under 980, 98 and 9.8 mN tension (Figs. 7(a), 8(a), and 9(a)), the bottom area is distorted by the initial imperfections. This is because a shape of a rigid membrane

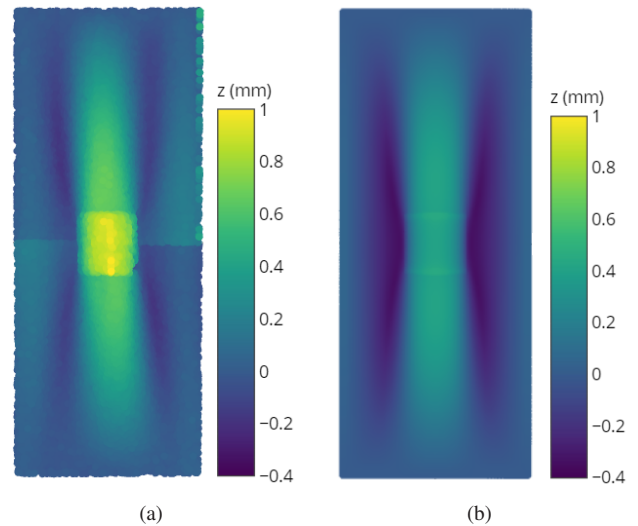


Fig. 6. Shapes of membrane with curved thin-film solar cell under 9800 mN tension. (a) Experiment. There is a joint line at the center of the membrane because the top half and bottom half of the membrane are simply connected. (b) Simulation.

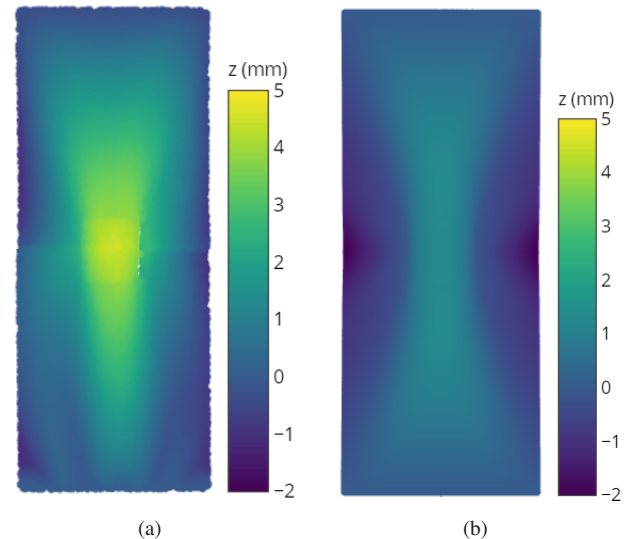


Fig. 7. Shapes of membrane with curved thin-film solar cell under 980 mN tension. (a) Experiment. There is a joint line at the center of the membrane because the top half and bottom half of the membrane are simply connected. (b) Simulation.

is insensitive to initial imperfections; the stronger the tension force is, the more rigid the membrane becomes.

In the experimental data, errors occurred. There is a joint line at the center of the membrane in each contour plot because the top half and bottom half of the membrane are simply connected. There is also holes in the cell, which are lack of measurement data because of specular reflection.

#### 5.1.1. Cross section

Figure 10 plots cross sections of the membrane with the cell at horizontal center lines of the membrane and the cell under each tension in the experiments and the simulations. Few 3D points are on the cross sections ( $y = 0$  mm) in a precise mathematical sense. Therefore, 3D points were plotted on the graph when their  $y$  components fell within the range of -0.1 mm to 0.1 mm. The range was chosen to make the cross section shape



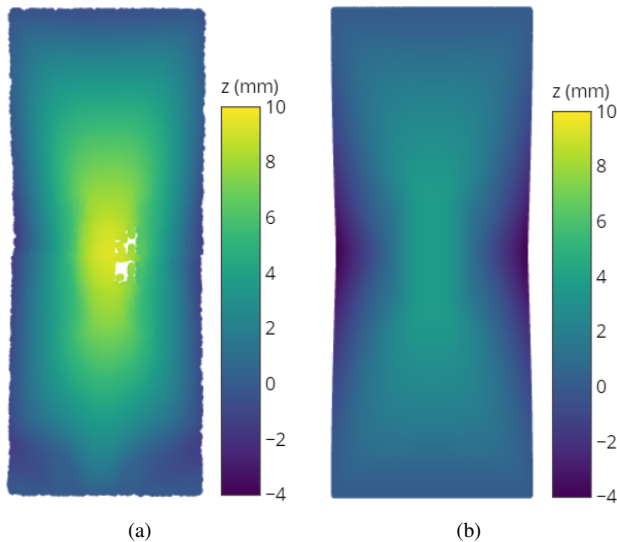


Fig. 8. Shapes of membrane with curved thin-film solar cell under 98 mN tension. (a) Experiment. Holes in the cell are lack of data. (b) Simulation.

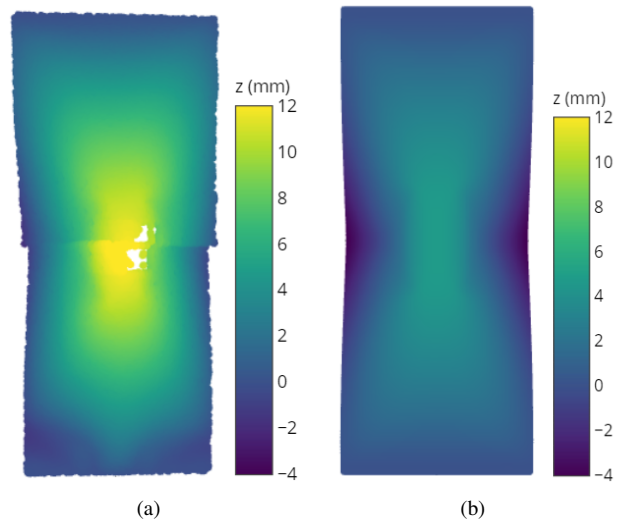


Fig. 9. Shapes of membrane with curved thin-film solar cell under 9.8 mN tension. (a) Experiment. Holes in the cell are lack of data. There is a joint line at the center of the membrane because the top half and bottom half of the membrane are simply connected. (b) Simulation.

clear and smooth. The cross sections of the simulations are globally similar to those of the experiments under each tension. The  $z$  of the simulations is the same as that of the experiments in the order of magnitude. A part of the numerical cross sections quantitatively matches the experimental cross sections. The stronger the tension force is, the better the numerical cross section corresponds with the experimental cross section. The numerical cell part matches the measured cell part better than the membrane part. This may be because the cell part has higher out-of-plane stiffness than the membrane part. In the measured membrane under 9800 mN tension, the initial curl of the membrane is particularly notable at the both ends ( $x < -40$  mm and  $40$  mm  $< x$ ).

### 5.1.2. Relationship between tension force and peak-to-peak out-of-plane position

Figure 11 plots the relationship between tension force and peak-to-peak  $z$  at the cross sections in the experiments and the

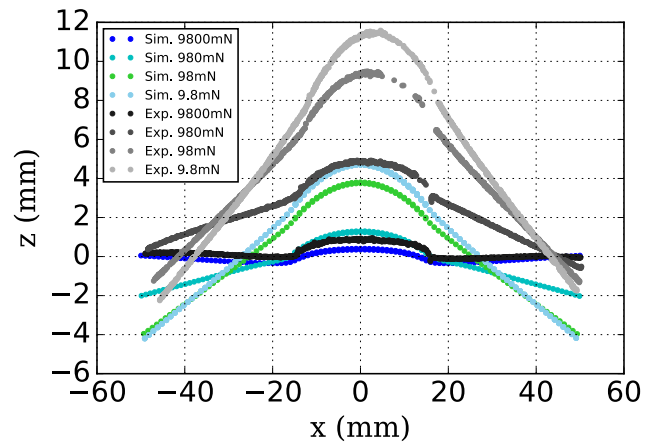


Fig. 10. Cross sections of membrane with curved thin-film solar cell at horizontal center line under each tension in experiments and simulations. The cross sections of the cells are in  $-15$  mm  $< x < 15$  mm. The measured cross sections of the membranes under 980, 98 and 9.8 mN tension missed in approximately  $0$  mm  $< x < 15$  mm because of specular reflection on the surface of the cell.

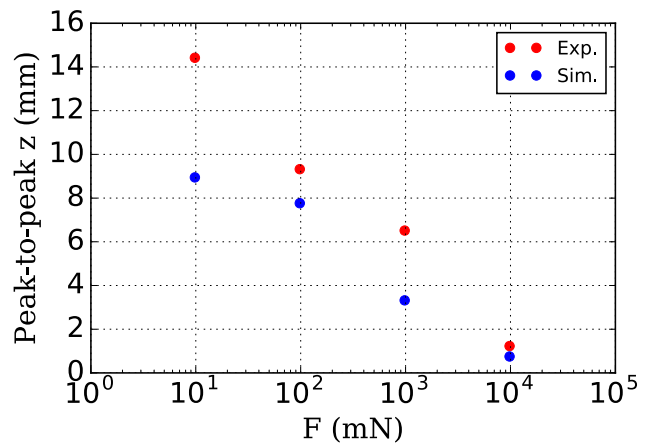


Fig. 11. Relationship between tension force and peak-to-peak out-of-plane position,  $z$  on cross sections at horizontal center lines of membrane and cell in experiments and simulations.

simulations. Peak-to-peak  $z$  means the length between the maximum and the minimum  $z$  of the cross section. Weak tension force makes peak-to-peak  $z$  increased because of low geometric stiffness. In case of weak force, curvature of the cell has a dominant influence on  $z$ . There might be a linear relationship between the log of tension force and peak-to-peak  $z$ . Peak-to-peak  $z$  of the measured membrane is larger than that of numerical membrane under each tension force. This may be due to the initial imperfections and the imperfect rigid boundary conditions of the top and bottom edges of the membrane in the experiments.

### 5.2. Maximum principal stress in simulation

Figure 12 shows the maximum in-plane principal stress on the neutral planes of the cross section at the horizontal center lines of the membrane and the cell under each tension force in the simulations. In  $-15$  mm  $< x < 15$  mm, the upper curves are the stress of the cells. The others are the stress of the membranes. In the simulation under 9800 mN tension (1.96 MPa stress), the shape of the membrane is stable due to the large tension; the maximum principal stress of the membrane in  $x <$

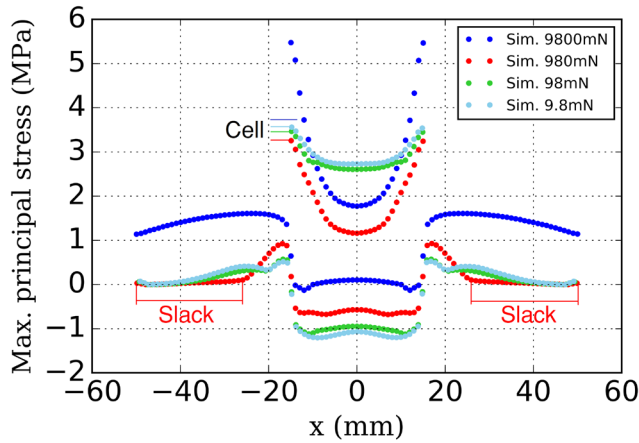


Fig. 12. Maximum in-plane principal stress on neutral planes of cross sections at horizontal center lines of membrane and cell under each tension force in simulations.

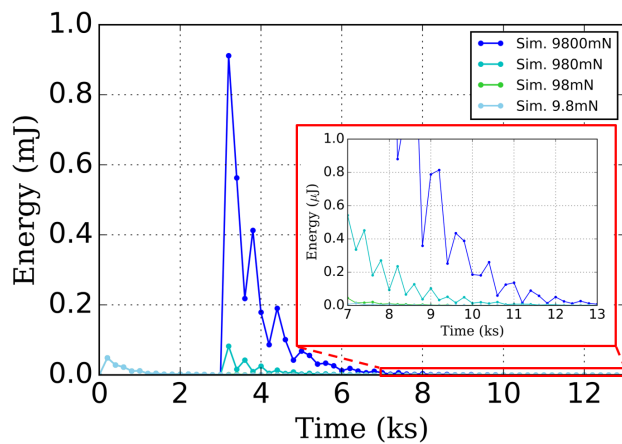


Fig. 13. Kinematic energy variation of whole membrane and cell in simulations.

-15 mm and  $15 \text{ mm} < x$  is more than 1 MPa, which is different from the others. In the simulation under 98 and 9.8 mN tension (0.0196 and 0.00196 MPa), the shapes of the membranes are also stable due to the small tension and curvature of the cell; the relatively slack section is small and the sign of the curvature is fixed. In the simulation under 980 mN tension (0.196 MPa), stress concentrates around the edges of the cell, and the large slack section is in  $x < -25 \text{ mm}$  and  $25 \text{ mm} < x$ . The shape of the slack region beside the cell is unstable; the surface can be concave or convex.

### 5.3. Kinematic energy variation

Figure 13 shows kinematic energy variation of the whole model in the simulations. Although the time increment is approximately 0.005 s, kinematic energy is plotted at intervals of 200 s. Because kinematic energies are under  $0.1 \mu\text{J}$  and gradients are low at the end of the simulations, the explicit dynamic analysis results are sufficiently close to steady-state at the end.

## 6. Conclusion

We measured and simulated wrinkles in the membrane with the curved cell under tension force as a simplified model of a part of the spinning solar power sail. The numerical shapes qualitatively match the measured shapes, and the out-of-plane

position of the numerical membranes is the same as that of the measured membranes in the order of magnitude. Therefore, the finite element model was qualitatively verified by the experiments. Wrinkle lines near both lateral sides of the curved cell are bent by curvature of the cell and become the X-shape. The X-shape occurs even if tension force on the membrane is changed.

Future work will include vibration experiments in order to investigate the relationship between out-of-plane stiffness and deformation of the membrane with the curved cell.

## Acknowledgments

This work was supported by JSPS KAKENHI Grant Number 26289329 and the JAXA/ISAS Solar Power Sail Preparation Team.

## References

- 1) Mori, O., Shirasawa, Y., Mimasu, Y., Tsuda, Y., Sawasda, H., Saiki, T., Yamamoto, T., Yonekura, K., Hoshino, H., and Kawaguchi, J.: Overview of IKAROS Mission, *Advances in Solar Sailing*, Macdonald, M. (ed.), Springer Berlin Heidelberg, Berlin and Heidelberg, 2014, pp. 25–43.
- 2) Satou, Y., Mori, O., Okuizumi, N., Shirasawa, Y., Furuya, H., and Sakamoto, H.: Deformation Properties of Solar Sail IKAROS Membrane with Nonlinear Finite Element Analyses, AIAA Paper 2015-0436, 2015.
- 3) Okuizumi, N., Satou, Y., Mori, O., Furuya, H., Sakamoto, H., and Shirasawa, Y.: Deployed Shape Analysis of Solar Power Sail Membrane, 57th JSASS/JSME/JAXA Structures Conference, Okayama, Japan, JSASS-2015-3068, 2015 (in Japanese).
- 4) Wong, Y. W., Pellegrino, S., and Park, K. C.: Prediction of Wrinkle Amplitudes in Square Solar Sails, AIAA Paper 2003-1982, 2003.
- 5) Senba, A., Ogi, Y., and Kogiso, N.: Wrinkle/Slack Control Using Shape Memory Polymer Films for Large Membrane Structures, AIAA Paper 2013-1928, 2013.
- 6) Hoang, B., White, S., Spence, B., and Kiefer, S.: Commercialization of Deployable Space Systems' Roll-Out Solar Array (ROSA) Technology for Space Systems Loral (SSL) Solar Arrays, 37th IEEE Aerospace Conference, Big Sky, USA, 978-1-4673-7676-1/16, 2016.
- 7) Wong, Y. W. and Pellegrino, S.: Wrinkled Membranes Part III: Numerical Simulations, *Journal of Mechanics of Materials and Structures*, **1** (2006), pp. 61–93.
- 8) Abaqus Analysis User's Guide (2016), <http://50.16.225.63/v2016/books/usb/default.htm> (accessed June 18, 2017).
- 9) Matsushita, M., Mori, O., Okuizumi, N., Satou, Y., Iwasa, T., and Matunaga, S.: Wrinkles in a Membrane with a Small Thin Film with Different Stiffness under Tension Load: Experiments and Simulations, 4th International Symposium on Solar Sailing, Kyoto, Japan, 17069, 2017.